NeuroImage: Clinical 34 (2022) 102985

Contents lists available at ScienceDirect

NeuroImage: Clinical

journal homepage: www.elsevier.com/locate/ynicl

Simultaneous assessment of regional distributions of atrophy across the neuraxis in MS patients

Patrick Freund [a,b,1,*], Nico Papinutto [c,1], Antje Bischof [c], Michela Azzarito [a], Gina Kirkish [c], John Ashburner [b], Alan Thompson [d], Stephen L. Hauser [c], Roland G. Henry [c]

[a] Spinal Cord Injury Center Balgrist, University Hospital Zurich, University of Zurich, Zurich, Switzerland
[b] Wellcome Centre for Human Neuroimaging, UCL Queen Square Institute of Neurology, University College London, London, United Kingdom
[c] UCSF Weill Institute for Neurosciences, Department of Neurology, University of California San Francisco, San Francisco, CA, USA
[d] Departments of Neuroinflammation, UCL Queen Square Institute of Neurology, University College London, London, United Kingdom

A B S T R A C T

Background: The ability to assess brain and cord atrophy simultaneously would improve the efficiency of MRI to track disease evolution.
Objective: To test a promising tool to *simultaneously* map the regional distribution of atrophy in multiple sclerosis (MS) patients across the brain and cord.
Methods: Voxel-based morphometry combined with a statistical parametric mapping probabilistic brain-spinal cord (SPM-BSC) template was applied to standard T1-weighted magnetic resonance imaging (MRI) scans covering the brain and cervical cord from 37 MS patients and 20 healthy controls (HC). We also measured the cord area at C2-C3 with a semi-automatic segmentation method using (i) the same T1-weighted acquisitions used for the new voxel-based analysis and (ii) dedicated spinal cord phase sensitive inversion recovery (PSIR) acquisitions. Cervical cord findings derived from the three approaches were compared to each other and the goodness to fit to clinical scores was assessed by regression analyses.
Results: The SPM-BSC approach revealed a severity-dependent pattern of atrophy across the cervical cord and thalamus in MS patients when compared to HCs. The magnitude of cord atrophy was confirmed by the semi-automatic extraction approach at C2-C3 using both standard brain T1-weighted and advanced cord dedicated acquisitions. Associations between atrophy of cord and thalamus with disability and cognition were demonstrated.
Conclusion: Atrophy in the brain and cervical cord of MS patients can be identified simultaneously and rapidly at the voxel-level. The SPM-BSC approach yields similar results as available standard processing tools with the added advantage of performing the analysis simultaneously and faster.

1. Introduction

MS is an inflammatory demyelinating disease (Lassmann, 2019) where focal brain and cord lesions produce disability (Filippi et al., 2012). Resulting symptoms include cognitive, visual, sensorimotor and autonomic impairment (Lublin et al., 2020). Progressive neurodegeneration (Schmierer et al., 2004) resulting in brain, particularly deep gray matter atrophy (e.g. thalamus) (Eshaghi et al., 2018) and cord atrophy (Eden et al., 2019; Valsasina et al., 2012), is a prominent component. Its accumulation over time is associated with the accrual of disability (Geurts et al., 2012), and although present in patients throughout the course of MS it is more severe in progressive MS patients and those transitioning to a progressive form of the disease (Bischof et al., 2022; Casserly et al., 2018; Fisniku et al., 2008). However, while the clinical eloquence of spinal involvement is recognized (Ciccarelli et al., 2019; Kearney et al., 2015b; Kearney et al., 2014; Lukas et al., 2015; Rocca et al., 2017; Schlaeger et al., 2014), clinical trials typically report only on neuroimaging outcome measures above the foramen magnum, such as number of brain lesions and global brain volume changes. Indeed, the implementation of harmonized spinal cord advanced acquisitions in the large number of centers usually involved in MS clinical trials is technically challenging and adds acquisition time to the scan session, not ideal for both the clinical trial sponsor and the patients. Reporting topographically defined atrophy measures simultaneously in the brain and spinal cord at the voxel-level using standard brain acquisitions extended to the upper cervical cord could impact clinical trials by enhancing sensitivity to disease related changes, reducing between-centre differences, improving the utility of MRI to track disease evolution in the real-world setting, and also increasing patients' comfort by reducing scan time. The development of a probabilistic brain and spinal cord (BSC) template (Blaiotta et al., 2018) – that is embedded in the SPM framework – now enables the simultaneous assessment of structural changes in the brain and cervical cord by using standard brain T1-weigthed acquisitions extended to the upper cervical

* Corresponding author.
E-mail address: patrick.freund@balgrist.ch (P. Freund).
[1] These first authors contributed equally to this work.

https://doi.org/10.1016/j.nicl.2022.102985
Received 1 December 2021; Received in revised form 5 March 2022; Accepted 7 March 2022
Available online 8 March 2022

spinal cord (Azzarito et al., 2020). In this study we assess this user friendly and fully automated approach (i) to address its clinical validity in MS patients, and (ii) to compare atrophic changes in the cervical cord and their goodness to fit to clinical scores against standard approaches of measuring total cross-sectional area (CSA) at the cervical level C2-C3 from phase sensitive inversion recovery (PSIR) images (Olney et al., 2018; Papinutto et al., 2015; Papinutto and Henry, 2019; Schlaeger et al., 2014) and from the same T1-weigthed scans used for the voxel-based approach (Liu et al., 2015; Papinutto et al., 2020b; Papinutto et al., 2018).

2. Subjects and methods

2.1. Standard protocol approvals, registrations, and patient consents

The Committee on Human Research at the University of California, San Francisco (UCSF) approved the study protocol and written informed consent was obtained from all participants.

2.1.1. Primary research question

The primary research question of this study was to assess the validity of simultaneous voxel-based morphometry measures to assess brain and spinal cord volume decreases.

2.1.2. Classification of evidence

This study provides Class II evidence that brain and cord atrophy can be reliably captured with the proposed voxel based morphometry (VBM) approach and that patients with the secondary progressive form of MS show more atrophy than relapsing remitting patients.

2.1.3. Participants and study design

Thirty-seven patients with a preexisting diagnosis of MS according to the revised McDonald criteria (20 relapsing remitting -RR-, 17 secondary progressive -SP-) and 20 healthy controls (HC) with no history of psychiatric, neurological, or cognitive disease were recruited. Demographic and clinical characteristics of the participants in the study are reported in Tables 1 and 2.

Table 1
Subjects' demographic and main clinical characteristics. Note, that age is statistically different ($p < 0.05$) when comparing healthy controls with multiple sclerosis patients (but not when comparing RR patients vs SP patients) while sex is not different across all the different groups.

	Healthy controls	RR patients	SP patients
N	20	20	17
Age (years)			
Mean +/- SD	42.05 +/- 14.15	57.55 +/- 6.70	58.05 +/- 9.10
Q1/Median/Q3	26.5/45.5/53.5	52.25/56.50/64.25	55.00/59.00/64.50
Sex (F/M)	12/8	9/11	10/7
Disease Duration (years)	–	18.90 +/- 8.10	23.70 +/- 10.20
Mean +/- SD		12.00/17.50/23.00	14.50/21.00/30.50
Q1/Median/Q3			
EDSS			
Q1/Median/Q3	–	1.50/1.75/3.00	5.25/6.00/6.50
Range		1.00/5.00	3.00/6.50

Table 2
Summary of clinical scores of patients with multiple sclerosis.

	All patients (N = 37)	RR patients (N = 20)	SP patients (N = 17)
EDSS			
Q1/Median/Q3	1.50/4.00/6.00	1.50/1.75/3.00	5.25/6.00/6.50
Range	1.00/6.50	1.00/5.00	3.00/6.50
MSSS			
Q1/Median/Q3	0.85/2.95/5.30	0.65/0.90/2.25	3.50/5.35/6.40
Range	0.30/8.15	0.30/4.80	1.70/8.15
PASAT			
Q1/Median/Q3	43.00/52.50/57.50	48.75/53.5/58.00	34.50/46.5/56.00
Range	15/60	38/60	15/60
T25-FW (sec)			
Q1/Median/Q3	4.35/5.05/7.40	4.00/4.40/4.00	6.40/7.80/19.95
Range	3.20/32.40	3.20/7.40	4.45/32.40
9-HPT dominant arm (sec)			
Q1/Median/Q3	19.25/21.55/24.75	18.75/20.85/22.35	21.10/23.35/28.60
Range	16.00/33.60	16.00/29.50	17.95/33.60
9-HPT non-dominant arm (sec)	20.40/22.25/25.80	19.90/21.55/23.80	21.50/24.00/30.75
Q1/Median/Q3			
Range	17.20/54.50	17.20/28.10	17.75/54.50
SDMT			
Q1/Median/Q3	36.75/46.75/51.00	45.25/49.00/51.00	33.00/39.75/49.50
Range	24.50/92.50	30.00/92.50	24.50/66.00

2.1.4. Experimental design

Results obtained with the proposed SPM-BSC analysis were compared with those obtained using existing tools that solely assess the spinal cord. Therefore, MRI data were analysed in the following way:

1. SPM-BSC in brain and spinal cord: 3D T1-weighted brain acquisitions extended to the upper cervical cord were analysed with the proposed VBM pipeline implemented in SPM12 using a brain and spinal cord template enabling statistical analysis in the spinal cord and brain conjointly;
2. CSA at C2-C3 was obtained from (i) spine dedicated PSIR images and (ii) the same 3D T1-weighted brain acquisitions extended to the upper cervical cord used for the SPM-BSC approach.

2.1.5. MRI acquisition

All participants underwent MRI scanning on a Siemens 3T Skyra scanner using either a 20- or 64-channel head-neck coil, and a 32-channel spine coil. Participants were positioned on the scanner table and their glabella used as landmark to be moved to the scanner isocenter. A standard high resolution T1-weighted acquisition of the brain (sagittal 3D MPRAGE, 1 mm^3 resolution, 176 slices per slab, repetition time (TR)/echo time (TE)/inversion time (TI) = 2300/3/900 ms, flip angle = 9°, parallel imaging acceleration factor (iPAT) = 2, non selective inversion pulse, 2D gradient nonlinearity filter applied, acquisition time ~5:30 min) with a large field of view (FOV) extended to include the upper cervical cord (256 mm in the head-foot direction, 240 mm in the anterior-posterior direction) and a single slice 2D PSIR acquisition with an optimized protocol (axial in-plane resolution 0.78×0.78 mm^2, slice thickness 5 mm, matrix 256×256, TR/TE/TI = 4000/3.22/400 ms, flip angle = 10°, three averages, slice selective inversion pulse, 2D gradient nonlinearity filter applied, acquisition time: 1:50 min, magnitude and

phase sensitive images reconstructed) were acquired for each participant (Papinutto et al., 2015) and constitute the key protocols of the study. The 2D PSIR protocol was acquired at the C2-C3 intervertebral disc level. Example of PSIR and MPRAGE acquisitions obtained with both the 20- and 64-channel head-neck coils are reported in Supplementary Fig. 1. A standard brain FLAIR (Fluid-Attenuated Inversion Recovery), along with sagittal T2-weigthed, sagittal STIR (Short Tau Inversion recovery) and axial T2*-weighted MEDIC (Multiple Echo Recombined Gradient Echo) protocols were also acquired on the upper cervical cord. These acquisitions were used for lesion detection.

Main parameters of these protocols were:.

- Brain FLAIR: sagittal acquisition, 1 mm^3 resolution, TR/TE/TI = 5000/388/1800 ms, iPAT = 3, acquisition time ~4:45 min;
- Spinal cord sagittal T2-weigthed: 0.7×0.7×2.4 mm^3 resolution, TR/TE = 3000/88 ms, iPAT = 2, acquisition time ~ 0:45 min;
- Spinal cord sagittal STIR: 0.7×0.7×2.0 mm^3 resolution, TR/TE/TI = 5610/51/200 ms, flip angle = 150°, iPAT = 2, acquisition time ~2:45 min;
- Spinal cord axial MEDIC: 0.4×0.4×3.0 mm^3 resolution, TR/TE = 740/17 ms, flip angle = 30°, iPAT = 3, four combined echoes, acquisition time ~5:00 min.

2.1.6. Lesion filling

White matter (WM) lesions in MS can affect tissue segmentation spatial normalizations of MRI acquisitions. Even though the unified normalizations (Ashburner and Friston, 2005) used in SPM may be solid enough when the number and volume of lesions is modest (Crinion et al., 2007), we chose to replace the lesion voxel intensity values with values derived from the surrounding WM voxels (Gelineau-Morel et al., 2012; Guo et al., 2019; Magon et al., 2014; Pareto et al., 2016) in the brain and spinal cord on the 3D T1-weighted acquisitions using FSL's lesion-filling algorithm (version 6.0.0) (Battaglini et al., 2012). This requires a user-defined lesion mask and white matter mask to fill lesions with local white matter intensities. The brain portion of the T1-weighted lesion masks were derived from FLAIR lesion masks created from the lesion segmentation toolbox (LST) (https://www.applied-statistics.de/lst.html (Schmidt et al., 2012)), software package SPM12. LST lesion masks were rigidly registered to T1-weighted brain image using FLIRT and lesion mask boundaries were refined from T1-weighted image intensity using a mixed-model algorithm we developed. Our mixed-model algorithm creates a lesion probability map using a histogram of normal appearing white matter (lower half of white matter intensity histogram) and an ideal lesion histogram (upper half of lesion intensity histogram) that do not overlap. The lesion probability map was calculated by dividing the lesion histogram by the sum of the lesion and normal appearing white matter histogram. Once the lesion probability map was produced, lesion boundaries were adjusted and redefined. SIENAX (version 2.6) (Smith et al., 2002) was run to obtain white matter brain masks. Since no reliable automatic tools exist yet, lesions of the spinal cord portion of the images were manually segmented from the T1-weighted image by a single experienced operator (AB) using biplanar sagittal T2 and STIR and axial T2*-weighted MEDIC images of the cervical cord for lesion identification and confirmation. These binary masks were refined from T1-weighted image using normal appearing white matter intensity as done for brain lesions.

2.2. Image analysis

2.2.1. Brain-neck template

The BSC-SPM template (Blaiotta et al., 2018) encodes probabilities of voxels in aligned images belonging to each of a number of tissue types (Blaiotta et al., 2016). The current BSC-SPM template encodes seven tissue types and has a field of view that incorporates the brain and the first four cervical segments. This template is in alignment with the existing SPM12 tissue probability template according to a 12-parameter affine mapping (Azzarito et al., 2020).

2.2.2. VBM pipeline for the simultaneous analysis of brain and spinal cord

The BSC-SPM template was used to segment the T1-weighted structural MPRAGE images of each individual using the unified segmentation algorithm of the traditional VBM pipeline (Ashburner and Friston, 2005). The settings were such that a single Gaussian was used to model intensity distributions for gray matter (GM), WM, cerebrospinal fluid (CSF) and fat, whereas a mixture of three Gaussians was used to model intensities of each of the non-neural tissues, soft tissues and to a mixture of bone and air. Note that the GM/WM classification in the cervical cord was arbitrary due to its lack of GM/WM contrast. In order to assess morphological differences in the cervical cord, the native-space GM and WM tissue maps identified by the above segmentation were combined to form a neural tissue (NT) class. Then, the GM, WM and NT maps were spatially normalised to MNI space with Dartel (Ashburner, 2007), and modulated by the Jacobian determinants of the deformations (Good et al., 2001). Finally, isotropic Gaussian smoothing by 6 mm full width at half maximum was applied to the modulated tissue maps. The total intracranial volume (TICV) was computed from the sum of the gray matter, white matter, and CSF volumes (Ridgway et al., 2011).

2.2.3. Spinal cord cross-sectional area measurement

C2-C3 CSA was obtained from both the phase-sensitive reconstructed PSIR images and from the MPRAGEs. For the PSIRs, CSA was measured semi-automatically by a single operator (NP), that was blinded to the demographic and clinical characteristics of the cohort, using the Jim "cord finder" toolkit (Horsfield et al., 2010) with fixed settings (nominal cord diameter 8 mm, number of shape coefficients 24, order of longitudinal variation 12) after manual marker placement on the mid-sagittal WM, directly posterior to the gray commissure (Papinutto et al., 2015). All segmentations were visually assessed, and in the few cases in which a lesion was located at the edge of the cord and the segmentation was not believed to be correct, a small manual correction was performed. Minimal manual corrections (CSA increased 1–2.5 mm^2 after correction) were made to five of the 17 SP patients and two of the 20 RR patients' cord segmentations (19% of the whole MS patient cohort).

For the MPRAGEs, CSA was measured semi-automatically by the same operator (NP), analogously to previous work (Papinutto et al., 2020b; Papinutto et al., 2018). Briefly, the sagittal lesion filled MPRAGE was resampled on the axial plane creating a packet of five contiguous slices 1-mm thick centered at the C2-C3 intevertebral disc. CSA was measured semi-automatically on these five slices and the average value computed, using the Jim "cord finder" toolkit with the same settings used for the PSIRs, after manual marker placement at the cord center of each of the five slices. All segmentations were visually assessed, and in the few cases in which the segmentation was not believed to be correct, a small manual correction was performed. This occurred in three of the 17 SP patients and two of the 20 RR patients' cord segmentations (13.5% of the whole MS patient cohort).

On the PSIR images at C2-C3 vertebral level, the same operator manually measured the maximum anterior-posterior diameter and lateral diameter of the spinal canal. The product of anterior-posterior canal diameter and lateral canal diameter was computed as a surrogate measure of the canal area (Papinutto et al., 2020a).

2.2.4. Clinical assessment

In MS patients, the Expanded Disability Status Scale (EDSS) and Multiple Sclerosis Severity Score (MSSS) at MRI visit were available for all 37 MS patients, while Timed 25-Foot Walk (T25-FW), 9-Hole Peg Test (9-HPT), Paced Auditory Serial Addition Test (PASAT) and Symbol Digit Modalities Test (SDMT) scores were available for all patients but one (36).

2.3. Statistical analyses

2.3.1. Morphometric assessments in the brain and spinal cord

To assess voxel-wise volumetric differences in the brain and spinal cord of MS patients compared to healthy controls, separate ANOVAs for the brain and cord were constructed with group (different MS subtypes and HCs) as the main factor within the framework of the multiple linear regression model of SPM. Age, sex, TICV and canal area were included as covariates of no interest for the spinal cord analyses. This was done because CSA has been found to depend on sex, TICV and canal area in a group of 129 healthy subjects (Papinutto et al., 2020a). Only the first three metrics were instead included as covariate for the brain analyses. Moreover, to increase sensitivity we also performed a region of interest (ROI) analysis in the deep gray matter (e.g. thalamus) (Eshaghi et al., 2018) based on extracted binary template files derived from the Anatomy toolbox (Eickhoff et al., 2005). We additionally used SPM's multiple linear regression models to test for associations between cord and brain changes and clinical outcomes in patients adjusting for potentially confounding effects of age, sex, TICV and canal area. A family-wise error (FWE) correction using Gaussian random field theory was applied to account for multiple comparisons (Friston et al., 1994) using a threshold of $p = 0.05$ at the peak-level, using either cord only or GM/WM brain masks in the different sub-analyses. The upper boundary of the spinal cord was defined as the first slice in the inferior direction that does not contain parts of the cerebellum, while the lower boundary was set to the last slice in inferior direction with reliable cord segmentation after visual inspection. Only statistically significant results at the peak level ($p < 0.05$) corrected for FWE are reported.

2.3.2. Cord area assessment from PSIRs and MPRAGEs

All statistical analyses were performed with JMP Pro 14 (https://www.jmp.com/en_ph/software/new-release/new-in-jmp-and-jmp-pro.html). Standard least squares models were used to explore correlations of CSA derived from PSIRs with EDSS and MSSS and to compare CSA among the different MS subtypes and HCs adjusting for age, sex, TICV and canal area as covariates, with disease duration (DD) included when assessing correlations with EDSS in patients.

To directly compare results obtained with the standard CSA methods against those from the BSC-SPM approach in the spinal cord, we extracted the value of the voxel of the smoothed and spatially normalized images in which voxel-wise association with EDSS was the highest. This value was plotted against the CSA semi-automatically measured from the PSIR and MPRAGE images. Moreover, the association between the semi-automatically derived CSA and EDSS and between CSA extracted from PSIRs and MPRAGEs was assessed by means of a Pearson correlation.

3. Results

3.1. Assessing brain and cervical cord atrophy at the voxel-level

At the level of the spinal cord, MS patients showed decreased cord volume when compared to healthy controls (Fig. 1), adjusting for age, sex, TICV, and canal area ($p_{FWE\text{-}corr} = 0.009$; $z = 3.7$; xyz (mm) = (0, −51, −97)). This effect was mainly driven by the SP patients, who showed a greater cord volume decrease when compared to RR patients ($p_{FWE\text{-}corr} = 0.01$; $z = 3.8$; xyz (mm) = (0, −52.5, −88)) and HC ($p_{FWE\text{-}corr} = 0.001$; $z = 4.3$; xyz (mm) = (0, −51, −97) and $p_{FWE\text{-}corr} = 0.03$; $z = 3.5$; xyz (mm) = (4.5, −58.5, −130)), adjusting for age, sex, TICV, and canal area. No statistically significative differences were detected between RR patients and HCs.

No differences were detected at the whole brain level with the SPM-BSC approach between MS patients and healthy controls. Within the ROI of the thalamus we found that MS patients showed atrophy in the thalamus bilaterally (left: $p_{FWE\text{-}corr} = 0.02$; $z = 3.9$ xyz (mm) = (15, −31.5, 3.5); right: $p_{FWE\text{-}corr} = 0.03$; $z = 3.8$ xyz (mm) = (-12, −34.5, 5)), adjusted for age, sex and TICV. This difference was driven by SP patients (left: $p_{FWE\text{-}corr} = 0.03$; $z = 3.7$ xyz (mm) = (13.5, −31.5, 5); right: $p_{FWE\text{-}corr} = 0.06$; $z = 3.5$; xyz (mm) = (-12, −34.5, 5)). However, there was no difference between SP and RR patients. No white matter volume differences were observed.

3.2. Cord area assessment from PSIRs and MPRAGEs

In standard least squares models, CSA of the 37 MS patients extracted from PSIRs had a significant negative correlation with EDSS, MSSS and T25-FW ($p = 0.0022$, $p = 0.0093$ and $p = 0.0202$ respectively, using also age, sex, TICV, and canal area in the model, and additionally DD for EDSS analyses). For the comparisons among the different MS subtypes and HCs, the standard least squares model including age, sex, TICV, and canal area, gave the following results for the effect of the group: HC vs all MS patients: $p = 0.0017$, HC vs RR patients: $p = 0.090$, HC vs SP patients: $p < 0.0001$, RR vs SP patients: $p = 0.0022$. Using bivariate fits (see Fig. 4), the CSA semi-automatically derived from PSIRs and MPRAGEs showed an inverse correlation with EDSS ($r = -0.52$ for both the acquisitions) and a high correlation with the voxel value of the smoothed and spatially normalized image found to have the highest correlation with EDSS in the SPM-BSC approach ($r = 0.81$ for PSIR, $r =$

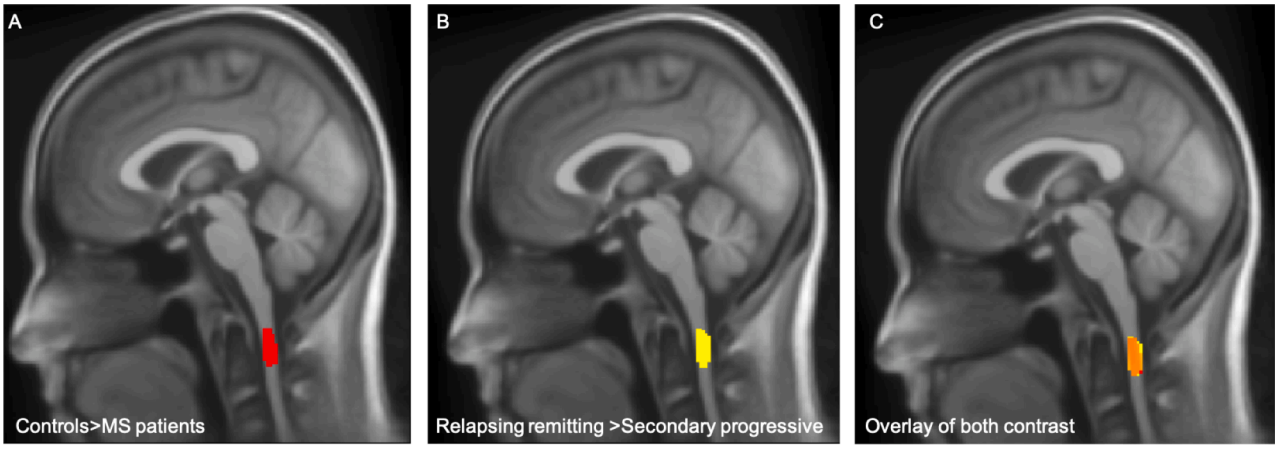

Fig. 1. Overlay of statistical parametric maps (uncorrected $p < 0.001$, for illustrative purposes) showing differences in MS patients compared to healthy controls (A), and between secondary progressive and relapsing remitting MS patients (B) in the cervical spinal cord based on the SPM-BSC approach. C shows the spatial overlap of the contrast healthy controls > MS patients (red) and relapsing remitting > secondary progressive MS patients (yellow). (For interpretation of the references to colour in this figure legend, the reader is referred to the web version of this article.)

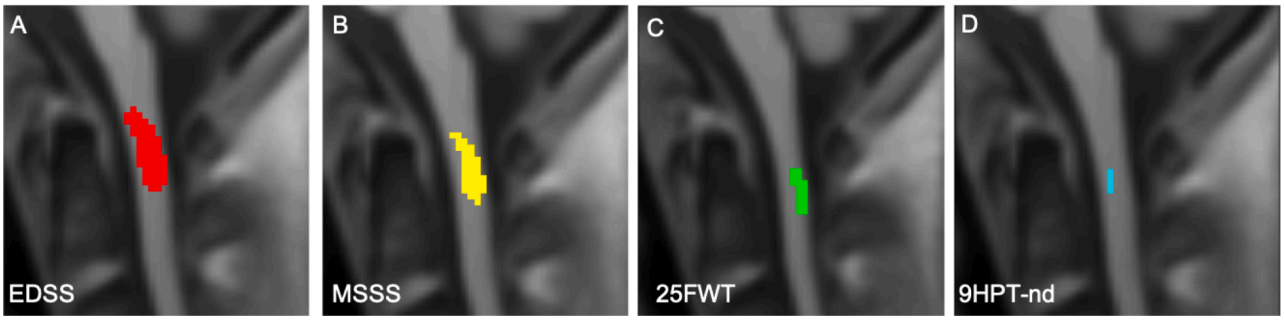

Fig. 2. Associations between clinical measures and spinal cord volume maps pre-processed using SPM-BSC. A significant association was found between worse EDSS (A), MSSS (B), 25FWT (C), 9HPT-nd (D) and cervical atrophy.

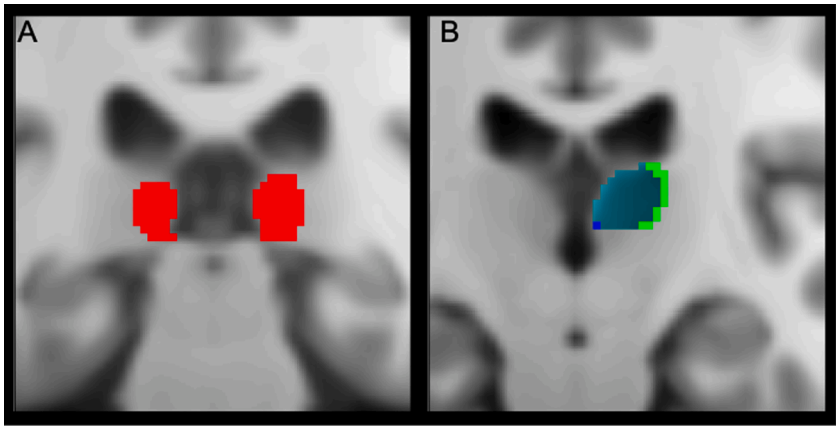

Fig. 3. Overlay of statistical parametric maps (uncorrected $p < 0.001$, for illustrative purposes) showing (A) differences (red) in MS patients compared to healthy controls in the bilateral Thalamus based on the SPM-BSC approach. (B) Green indicates an association between worse SDMT score and greater right thalamic atrophy (blue). (For interpretation of the references to colour in this figure legend, the reader is referred to the web version of this article.)

0.84 for MPRAGE). CSA extracted form PSIRs and MPRAGEs were highly correlated ($r = 0.96$, see Supplementary Fig. 2).

3.3. Correlation analysis with the SPM-BSC approach

In the spinal cord data, we found that a lower volume was associated with higher EDSS ($p_{FWE\text{-}corr} = 0.007$; $z = 3.8$; xyz (mm) = (3, −50, −102) and $p_{FWE\text{-}corr} = 0.031$; $z = 3.7$; xyz (mm) = (5, −59, −132)) and MSSS ($p_{FWE\text{-}corr} = 0.001$; $z = 4.3$; xyz (mm) = (0, −53, −88) and $p_{FWE\text{-}corr} = 0.005$; $z = 3.9$; xyz (mm) = (5, −59, −122)) (Fig. 2).

In the GM ROI of the thalamus, we found an association between a lower right thalamic volume and higher SDMT (Fig. 3) ($p_{FWE\text{-}corr} = 0.013$; $z = 4.05$, xyz (mm) = (15, −27, 8)). We did not find any associations in the WM of the brain (Fig. 3).

4. Discussion

This study demonstrates the feasibility of a combined brain and spinal cord voxel-based analysis approach in MS patients and healthy controls within the SPM12 framework using standard brain MRI acquisitions extended to the upper cervical cord. This was achieved by investigating the between-group effect of MS patients and healthy controls and correlations with clinical scores on MRI data in the brain and in the spinal cord using the new SPM-BSC analysis and by comparing the spinal cord results with a CSA analysis based on PSIR spine dedicated images and on the same MPRAGEs used for brain analyses. The SPM-BSC proved sensitive to detect disease-associated effects in the small cohort under investigation that were remarkable in the spinal cord and moderate in the brain.

Voxel-wise analysis in the brain and spinal cord using the SPM-BSC approach showed regional atrophy in patients when compared to healthy controls, which was evident in the spinal cord and only to a limited extent in the brain (thalamus only). The magnitude of cord atrophy was comparable to conventional analysis using CSA derived from spinal cord dedicated acqusitions and T1-weigthed brain acquisitions extended to the upper cervical cord. SPM-BSC and CSA from PSIR showed a remarkable degree of atrophy in the spinal cord. There was no difference in the atrophic changes in the spinal cord observed with the SPM-BSC and CSA approaches when comparing HC with RR patients, but major differences when comparing HC and RR patients with SP patients, in line with the literature (Kearney et al., 2015a; Schlaeger et al., 2014). This demonstrates that the SPM-BSC approach can detect pathology-related differences at the voxel level between MS patients and healthy controls using brain T1-weighted images extended to the spinal cord, similarly to existing acquisitions and processing tools dedicated to the spinal cord only. While both the CSA and SPM-BSC approaches showed consistent associations with clinical impairment scales (i.e. EDSS and MSSS), the voxel-based nature of the SPM-BSC approach showed not only that voxels at the C2-C3 level were associated with the degree of impairment, but that these clusters also included the cervical C1 segment, where associations were even stronger (Bischof et al., 2022). Crucially, the extent of regional atrophy was overlapping with the identified cluster revealed by the correlations, indicating its clinical validity.

Previous literature has indicated that thalamus is affected by atrophy, starting from the early stages of the disease (Blinkenberg et al., 2000; Fabiano et al., 2003). The spatial overlap between atrophic changes in the right thalamus and the association between the latter with SDMT underlines the fact that the SPM-BSC approach is also sensitive to brain changes. The simultaneous brain/cervical cord analysis

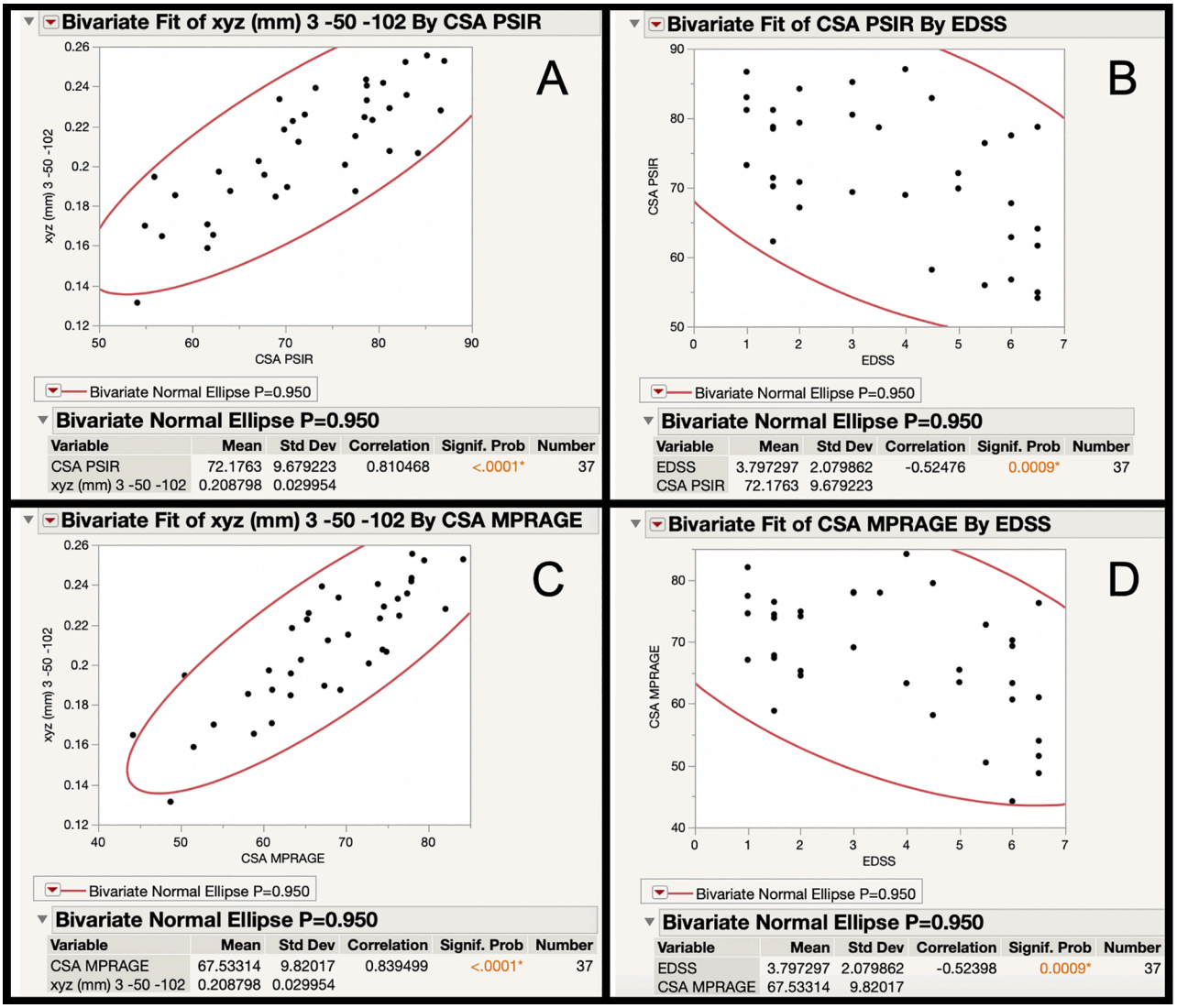

Fig. 4. Correlations between voxel-based and total cross-sectional area (CSA) measurements (A: derived from PSIR, C: derived from MPRAGE) and between CSA and EDSS (B: derived from PSIR, D: derived from MPRAGE).

allowed detection of correlations with clinical scores driven by motor symptoms (EDSS and MSSS) located in the upper cervical cord, while cognitive measures correlated with volume changes in the thalamus. This finding is in line with previous studies that suggest that spinal cord atrophy has generally a stronger correlation with patient disability measured in terms of EDSS than brain atrophy (Rocca et al., 2017).

MS lesions influence tissue segmentation and spatial normalizations (Gelineau-Morel et al., 2012; Guo et al., 2019; Magon et al., 2014; Pareto et al., 2016). Thus, performing or not performing lesion filling could influence the sensitivity to detect a difference (in terms of type I and type II errors) depending on the study's statistical power from sample size. Evaluating which is the best way of dealing with lesions was beyond the scope of this study, therefore we decided to adopt a lesion filling method in line with some of the most recent works in the MS field (Gelineau-Morel et al., 2012; Guo et al., 2019; Magon et al., 2014; Pareto et al., 2016).

This study has some limitations. Firstly, the BSC template covers only the first four cervical segments. However, a template including more caudal parts of the spinal cord is envisioned as part of future work using a related algorithm (Brudfors et al., 2020) and will be available with the next set of SPM12 updates. Secondly, the GM/WM classification in the spinal cord based on the T1-weighted scans is arbitrary due to lack of contrast. Thus, we summed up the probability maps of GM and WM to generate a probability map of NT, which is a non-specific measure of spinal cord volume.

Two different head-neck coils were used to acquire the MRI data. However, Supplementary Fig. 1 shows that the quality of images acquired with the different coils is consistent. Moreover, the distribution of coils used was consistent across the different groups of MS patients and HCs, therefore we believe results should not be significantly affected by a systematic bias resulting from different tissue segmentation due to differences in GM/WM contrast (Panman et al., 2019). A 3D filter to correct for gradient nonlinearity would be ideal when measuring spinal cord areas at the periphery of the FOV on MPRAGEs. However, a 2D filter combined with the consistent positioning of subjects – performed by a single MRI technologist at our center, using the glablella as landmark – render potential measurement errors (Papinutto et al., 2018) negligible, particularly considering the cross-sectional nature of this study. This was shown by the high correlation between CSA extracted from the PSIRs (at the scanner isocenter) and from the 2D corrected MPRAGEs (at the edges of the FOV).

Finally, the cohort under investigation was small, but we believe that it constitutes a reasonable representation in terms of demographic/clinical distribution, atrophy differences between the different sub-

groups, correlations of CSA values with EDSS and MSSS for the aims of this test of the SPM-BSC framework on MS patients. The small sample size of the cohort can explain the modest findings with the SPM-BSC approach in the brain, where atrophy is known to be widespread and of moderate extent when compared with the upper levels of the cervical spinal cord (Schlaeger et al., 2014). The SPM-BSC approach could also be slightly less sensitive in the brain when compared with the standard brain VBM approach, considering that a lower sensitivity was detected in the previous work on spinal cord injury patients (Azzarito et al., 2020; Kyathanahally et al., 2021). This is a single center study with small sample size, therefore further tests of the tool with larger datasets acquired with multiple scanners at multiple centers are warranted to test the feasibility of its usage in large clinical trials.

In conclusion, this study on MS patients provides the clinical validity of the SPM-BSC approach for the simultaneous analysis of the brain and cervical spinal cord atrophy measurements in the SPM framework. The proposed method using anatomical brain T1-weighted scans extended to the upper spinal cord (up to cervical level C4) yielded comparable results to more standard cord-specific approaches. Besides traumatic SCI (Azzarito et al., 2020) and MS, this method is applicable to MRI studies investigating any condition with suspected spinal cord involvement. This approach provides a means of assessing spatially distributed pathophysiological changes in the brain and spinal cord and their relationship with disability accumulation. The application to longitudinal brain and spinal cord MRI data of MS patients will be assessed in future studies.

Declaration of Competing Interest

The authors declare that they have no known competing financial interests or personal relationships that could have appeared to influence the work reported in this paper.

Acknowledgment

We are grateful to all participants of this study for their contribution and the time they invested in this study.

Study funding

PF is funded by a SNF Eccellenza Professorial Fellowship grant (PCEFP3_181362/1). Open access of this publication is supported by the Wellcome Trust (091593/Z/10/Z).

Author disclosures

Alan Thompson reports personal fees paid to his institution from Eisai Ltd and fees and support for travel from Hoffmann-La Roche outside the submitted work; and Editorial Board member, The Lancet Neurology, receiving free subscription; Editor-in-Chief, Multiple Sclerosis Journal, honorarium from SAGE Publications; support for travel as Chair, Scientific Advisory Committee, International Progressive MS Alliance, and member, National MS Society (USA), Research Programs Advisory Committee. Received honoraria and support for travel for lecturing from EXCEMED and Almirall. A.J.T. acknowledges also support from the UCL/UCLH NIHR Biomedical Research Centre.

Stephen L. Hauser: Reports service on the board of directors for Neurona and on scientific advisory boards for Annexon, Molecular Stethoscope, Bionure and Alector; and has received travel reimbursement and writing assistance from F Hoffmann-La Roche and Novartis AG for CD20-related meetings and presentations.

Roland G. Henry: Reports fees for consultation and advisory boards from Novartis, Roche/Genentech, Sanofi/Genzyme, Celgene, QIA, Medday, Atara, Neurona.

Appendix A. Supplementary data

Supplementary data to this article can be found online at https://doi.org/10.1016/j.nicl.2022.102985.

Table A1
Appendix.

Name	Location	Role	Contribution
Patrick Freund, MD, PhD	Balgrist University Hospital, Zurich	Author	Designed and conceptualized the study; acquired and analyzed the data; drafted the manuscript for intellectual content
Nico Papinutto, PhD	UCSF Weill Institute for Neurosciences, Department of Neurology, University of California San Francisco	Author	Study concept and design; acquisition, analysis, and interpretation of data; writing the manuscript
Antje Bischof, MD	UCSF Weill Institute for Neurosciences, Department of Neurology, University of California San Francisco	Author	Study concept and design; acquisition and analysis of data; critical revision of manuscript for intellectual content
Michela Azzaritto, PhD	Balgrist University Hospital, Zurich	Author	Study concept and design; critical revision of manuscript for intellectual content.
Gina Kirkish, MS	UCSF Weill Institute for Neurosciences, Department of Neurology, University of California San Francisco	Author	Data analysis; critical revision of manuscript for intellectual content
John Ashburner, PhD	Wellcome Centre for Human Neuroimaging, UCL Queen Square Institute of Neurology, University College London	Author	Study concept and design; critical revision of manuscript for intellectual content; study supervision.
Alan Thompson, MD	Department of Neuroinflammation, UCL Queen Square Institute of Neurology, University College London	Author	Study concept and design; critical revision of manuscript for intellectual content; study supervision.
Stephen Hauser, MD	UCSF Weill Institute for Neurosciences, Department of Neurology, University of California San Francisco	Author	Study concept and design; critical revision of manuscript for intellectual content; study supervision.
Roland Henry, PhD	UCSF Weill Institute for Neurosciences, Department of Neurology, University of California, San Francisco	Author	Study concept and design; critical revision of manuscript for intellectual content; study supervision

References

Ashburner, J., 2007. A fast diffeomorphic image registration algorithm. Neuroimage. 38, 95–113.
Ashburner, J., Friston, K.J., 2005. Unified segmentation. Neuroimage. 26, 839–851.
Azzarito, M., Kyathanahally, S.P., Balbastre, Y., Seif, M., Blaiotta, C., Callaghan, M.F., Ashburner, J., Freund, P., 2020. Simultaneous voxel-wise analysis of brain and spinal cord morphometry and microstructure within the SPM framework. Hum, Brain Mapp.
Battaglini, M., Jenkinson, M., De Stefano, N., 2012. Evaluating and reducing the impact of white matter lesions on brain volume measurements. Hum. Brain Mapp. 33, 2062–2071.
Bischof, A., Papinutto, N., Keshavan, A., Rajesh, A., Kirkish, G., Zhang, X., Mallott, J.M., Asteggiano, C., Sacco, S., Gundel, T.J., Zhao, C., Stern, W.A., Caverzasi, E., Zhou, Y., Gomez, R., Ragan, N.R., Santaniello, A., Zhu, A.H., Juwono, J., Bevan, C.J., Bove, R. M., Crabtree, E., Gelfand, J.M., Goodin, D.S., Graves, J.S., Green, A.J., Oksenberg, J. R., Waubant, E., Wilson, M.R., Zamvil, S.S., Cree, B.A.C., Hauser, S.L., Henry, R.G., 2022. Spinal Cord Atrophy Predicts Progressive Disease in Relapsing Multiple Sclerosis. Ann. Neurol. 91, 268–281.
Blaiotta, C., Freund, P., Cardoso, M.J., Ashburner, J., 2018. Generative diffeomorphic modelling of large MRI data sets for probabilistic template construction. Neuroimage 166, 117–134.

Blaiotta, C., Jorge Cardoso, M., Ashburner, J., 2016. Variational inference for medical image segmentation. Comput. Vis. Image Underst. 151, 14–28.
Blinkenberg, M., Rune, K., Jensen, C.V., Ravnborg, M., Kyllingsbaek, S., Holm, S., Paulson, O.B., Sorensen, P.S., 2000. Cortical cerebral metabolism correlates with MRI lesion load and cognitive dysfunction in MS. Neurology 54, 558–564.
Brudfors, M., Balbastre, Y., Flandin, G., Nachev, P., Ashburner, J., 2020. Flexible Bayesian Modelling for Nonlinear Image Registration. Lect. Notes Comput. Sci. (including Subser. Lect. Notes Artif. Intell. Lect. Notes Bioinformatics) 12263 LNCS, 253–263.
Casserly, C., Seyman, E.E., Alcaide-Leon, P., Guenette, M., Lyons, C., Sankar, S., Svendrovski, A., Baral, S., Oh, J., 2018. Spinal Cord Atrophy in Multiple Sclerosis: A Systematic Review and Meta-Analysis. J. Neuroimaging 28, 556–586.
Ciccarelli, O., Cohen, J.A., Reingold, S.C., Weinshenker, B.G., Amato, M.P., Banwell, B., Barkhof, F., Bebo, B., Becher, B., Bethoux, F., Brandt, A., Brownlee, W., Calabresi, P., Chatway, J., Chien, C., Chitnis, T., Cohen, J., Comi, G., Correale, J., De Sèze, J., De Stefano, N., Fazekas, F., Flanagan, E., Freedman, M., Fujihara, K., Galetta, S., Goldman, M., Greenberg, B., Hartung, H.P., Hemmer, B., Henning, A., Izbudak, I., Kappos, L., Lassmann, H., Laule, C., Levy, M., Lublin, F., Lucchinetti, C., Lukas, C., Marrie, R.A., Miller, A., Miller, D., Montalban, X., Mowry, E., Ourselin, S., Paul, F., Pelletier, D., Ranjeva, J.P., Reich, D., Reingold, S., Rocca, M.A., Rovira, A., Schlaerger, R., Soelberg Sorensen, P., Sormani, M., Stuve, O., Thompson, A., Tintoré, M., Traboulsee, A., Trapp, B., Trojano, M., Uitdehaag, B., Vukusic, S., Waubant, E., Weinshenker, B., Wheeler-Kingshott, C.G., Xu, J., 2019. Spinal cord involvement in multiple sclerosis and neuromyelitis optica spectrum disorders. Lancet Neurol.
Crinion, J., Ashburner, J., Leff, A., Brett, M., Price, C., Friston, K., 2007. Spatial normalization of lesioned brains: performance evaluation and impact on fMRI analyses. Neuroimage 37, 866–875.
Eden, D., Gros, C., Badji, A., Dupont, S.M., De Leener, B., Maranzano, J., Zhuoquiong, R., Liu, Y., Granberg, T., Ouellette, R., Stawiarz, L., Hillert, J., Talbott, J., Bannier, E., Kerbrat, A., Edan, G., Labauge, P., Callot, V., Pelletier, J., Audoin, B., Rasoanandrianina, H., Brisset, J.-C., Valsasina, P., Rocca, M.A., Filippi, M., Bakshi, R., Tauhid, S., Prados, F., Yiannakas, M., Kearney, H., Ciccarelli, O., Smith, S. A., Andrada Treaba, C., Mainero, C., Lefeuvre, J., Reich, D.S., Nair, G., Shepherd, T. M., Charlson, E., Tachibana, Y., Hori, M., Kamiya, K., Chougar, L., Narayanan, S., Cohen-Adad, J., 2019. Spatial distribution of multiple sclerosis lesions in the cervical spinal cord. Brain 142, 633–646.
Eickhoff, S.B., Stephan, K.E., Mohlberg, H., Grefkes, C., Fink, G.R., Amunts, K., Zilles, K., 2005. A new SPM toolbox for combining probabilistic cytoarchitectonic maps and functional imaging data. Neuroimage. 25, 1325–1335.
Eshaghi, A., Prados, F., Brownlee, W.J., Altmann, D.R., Tur, C., Cardoso, M.J., De Angelis, F., van de Pavert, S.H., Cawley, N., De Stefano, N., Stromillo, M.L., Battaglini, M., Ruggieri, S., Gasperini, C., Filippi, M., Rocca, M.A., Rovira, A., Sastre-Garriga, J., Vrenken, H., Leurs, C.E., Killestein, J., Pirpamer, L., Enzinger, C., Ourselin, S., Wheeler-Kingshott, C.A.M.G., Chard, D., Thompson, A.J., Alexander, D. C., Barkhof, F., Ciccarelli, O., 2018. Deep gray matter volume loss drives disability worsening in multiple sclerosis. Ann. Neurol. 83, 210–222.
Fabiano, A.J., Sharma, J., Weinstock-Guttman, B., Munschauer III, F.E., Benedict, R.H., Zivadinov, R., Bakshi, R., 2003. Thalamic involvement in multiple sclerosis: a diffusion-weighted magnetic resonance imaging study. J. Neuroimaging 13, 307–314.
Filippi, M., Rocca, M.A., Barkhof, F., Brück, W., Chen, J.T., Comi, G., DeLuca, G., De Stefano, N., Erickson, B.J., Evangelou, N., Fazekas, F., Geurts, J.J.G., Lucchinetti, C., Miller, D.H., Pelletier, D., Popescu, B.F.G., Lassmann, H., 2012. Association between pathological and MRI findings in multiple sclerosis. Lancet Neurol.
Fisniku, L.K., Chard, D.T., Jackson, J.S., Anderson, V.M., Altmann, D.R., Miszkiel, K.A., Thompson, A.J., Miller, D.H., 2008. Gray matter atrophy is related to long-term disability in multiple sclerosis. Ann. Neurol. 64, 247–254.
Friston, K.J., Worsley, K.J., Frackowiak, R.S., Mazziotta, J.C., Evans, a C.,, 1994. Assessing the significance of focal activations using their spatial extent. Hum. Brain Mapp. 1, 210–220.
Gelineau-Morel, R., Tomassini, V., Jenkinson, M., Johansen-Berg, H., Matthews, P.M., Palace, J., 2012. The effect of hypointense white matter lesions on automated gray matter segmentation in multiple sclerosis. Hum. Brain Mapp. 33, 2802–2814.
Geurts, J.J.G., Calabrese, M., Fisher, E., Rudick, R.A., 2012. Measurement and clinical effect of grey matter pathology in multiple sclerosis. Lancet Neurol.
Good, C.D., Johnsrude, I.S., Ashburner, J., Henson, R.N.A., Friston, K.J., Frackowiak, R.S. J., 2001. A voxel-based morphometric study of ageing in 465 normal adult human brains. Neuroimage. 14, 21–36.
Guo, C., Ferreira, D., Fink, K., Westman, E., Granberg, T., 2019. Repeatability and reproducibility of FreeSurfer, FSL-SIENAX and SPM brain volumetric measurements and the effect of lesion filling in multiple sclerosis. Eur. Radiol. 29, 1355–1364.
Horsfield, M., a, Sala, S., Neema, M., Absinta, M., Bakshi, A., Sormani, M.P., Rocca, M.A., Bakshi, R., Filippi, M.,, 2010. Rapid semi-automatic segmentation of the spinal cord from magnetic resonance images: application in multiple sclerosis. Neuroimage. 50, 446–455.
Kearney, H., Miller, D.H., Ciccarelli, O., 2015a. Spinal cord MRI in multiple sclerosis—diagnostic, prognostic and clinical value. Nat. Rev. Neurol. 11, 327–338.
Kearney, H., Rocca, M.A., Valsasina, P., Balk, L., Sastre-Garriga, J., Reinhardt, J., Ruggieri, S., Rovira, A., Stippich, C., Kappos, L., Sprenger, T., Tortorella, P., Rovaris, M., Gasperini, C., Montalban, X., Geurts, J.J.G., Polman, C.H., Barkhof, F., Filippi, M., Altmann, D.R., Ciccarelli, O., Miller, D.H., Chard, D.T., 2014. Magnetic resonance imaging correlates of physical disability in relapse onset multiple sclerosis of long disease duration. Mult. Scler. 20, 72–80.
Kearney, H., Schneider, T., Yiannakas, M.C., Altmann, D.R., Wheeler-Kingshott, C.A.M., Ciccarelli, O., Miller, D.H., 2015b. Spinal cord grey matter abnormalities are associated with secondary progression and Physical disability in multiple sclerosis. J. Neurol. Neurosurg. Psychiatry 86, 608–614.
Kyathanahally, S.P., Azzarito, M., Rosner, J., Calhoun, V.D., Blaiotta, C., Ashburner, J., Weiskopf, N., Wiech, K., Friston, K., Ziegler, G., Freund, P., 2021. Microstructural plasticity in nociceptive pathways after spinal cord injury. J. Neurol. Neurosurg. & Psychiatry jnnp-2020-325580.
Lassmann, H., 2019. Pathogenic mechanisms associated with different clinical courses of multiple sclerosis. Front, Immunol.
Liu, Z., Yaldizli, Ö., Pardini, M., Sethi, V., Kearney, H., Muhlert, N., Wheeler-Kingshott, C., Miller, D.H., Chard, D.T., 2015. Cervical cord area measurement using volumetric brain magnetic resonance imaging in multiple sclerosis. Mult. Scler. Relat. Disord. 4, 52–57.
Lublin, F.D., Coetzee, T., Cohen, J.A., Marrie, R.A., Thompson, A.J., 2020. The 2013 clinical course descriptors for multiple sclerosis. A clarification, Neurology.
Lukas, C., Knol, D.L., Sombekke, M.H., Bellenberg, B., Hahn, H.K., Popescu, V., Weier, K., Radue, E.W., Gass, A., Kappos, L., Naegelin, Y., Uitdehaag, B.M.J., Geurts, J.J.G., Barkhof, F., Vrenken, H., 2015. Cervical spinal cord volume loss is related to clinical disability progression in multiple sclerosis. J. Neurol. Neurosurg. Psychiatry 86, 410–418.
Magon, S., Gaetano, L., Chakravarty, M.M., Lerch, J.P., Naegelin, Y., Stippich, C., Kappos, L., Radue, E.W., Sprenger, T., 2014. White matter lesion filling improves the accuracy of cortical thickness measurements in multiple sclerosis patients: A longitudinal study. BMC Neurosci. 15, 106.
Olney, N.T., Bischof, A., Rosen, H., Caverzasi, E., Stern, W.A., Lomen-Hoerth, C., Miller, B.L., Henry, R.G., Papinutto, N., 2018. Measurement of spinal cord atrophy using phase sensitive inversion recovery (PSIR) imaging in motor neuron disease. PLoS One 13.
Panman, J.L., To, Y.Y., Van Der Ende, E.L., Poos, J.M., Jiskoot, L.C., Meeter, L.H.H., Dopper, E.G.P., Bouts, M.J.R.J., Van Osch, M.J.P., Rombouts, S.A.R.B., Van Swieten, J.C., Van Der Grond, J., Papma, J.M., Hafkemeijer, A., 2019. Bias introduced by multiple head coils in mri research: An 8 channel and 32 channel coil comparison. Front. Neurosci. 13, 729.
Papinutto, N., Asteggiano, C., Bischof, A., Gundel, T.J., Caverzasi, E., Stern, W.A., Bastianello, S., Hauser, S.L., Henry, R.G., 2020a. Intersubject Variability and Normalization Strategies for Spinal Cord Total Cross-Sectional and Gray Matter Areas. J. Neuroimaging 30, 110–118.
Papinutto, N., Bakshi, R., Bischof, A., Calabresi, P.A., Caverzasi, E., Constable, R.T., Datta, E., Kirkish, G., Nair, G., Oh, J., Pelletier, D., Pham, D.L., Reich, D.S., Rooney, W., Roy, S., Schwartz, D., Shinohara, R.T., Sicotte, N.L., Stern, W.A., Tagge, I., Tauhid, S., Tummala, S., Henry, R.G., 2018. Gradient nonlinearity effects on upper cervical spinal cord area measurement from 3D T1-weighted brain MRI acquisitions. Magn. Reson. Med. 79, 1595.
Papinutto, N., Cordano, C., Asteggiano, C., Caverzasi, E., Mandelli, M.L., Lauricella, M., Yabut, N., Neylan, M., Kirkish, G., Gorno-Tempini, M.L., Henry, R.G., 2020b. MRI Measurement of Upper Cervical Spinal Cord Cross-Sectional Area in Children. J. Neuroimaging 30, 598–602.
Papinutto, N., Henry, R.G., 2019. Evaluation of Intra- and Interscanner Reliability of MRI Protocols for Spinal Cord Gray Matter and Total Cross-Sectional Area Measurements. J. Magn. Reson. Imaging 49, 1078–1090.
Papinutto, N., Schlaeger, R., Panara, V., Caverzasi, E., Ahn, S., Johnson, K.J., Zhu, A.H., Stern, W.A., Laub, G., Hauser, S.L., Henry, R.G., 2015. 2D phase-sensitive inversion recovery imaging to measure in vivo spinal cord gray and white matter areas in clinically feasible acquisition times. J. Magn. Reson. Imaging 42, 698–708.
Pareto, D., Sastre-Garriga, J., Aymerich, F.X., Auger, C., Tintoré, M., Montalban, X., Rovira, A., 2016. Lesion filling effect in regional brain volume estimations: a study in multiple sclerosis patients with low lesion load. Neuroradiology 58, 467–474.
Ridgway, G., Barnes, J., Pepple, T., Fox, N., 2011. Estimation of total intracranial volume; a comparison of methods. Alzheimer's Dement. 7, S62–S63.
Rocca, M.A., Comi, G., Filippi, M., 2017. The Role of T1-Weighted Derived Measures of Neurodegeneration for Assessing Disability Progression in Multiple Sclerosis. Front, Neurol, p. 8.
Schlaeger, R., Papinutto, N., Panara, V., Bevan, C., Lobach, I.V., Bucci, M., Caverzasi, E., Gelfand, J.M., Green, A.J., Jordan, K.M., Stern, W.A., Von Büdingen, H.C., Waubant, E., Zhu, A.H., Goodin, D.S., Cree, B.A.C., Hauser, S.L., Henry, R.G., 2014. Spinal cord gray matter atrophy correlates with multiple sclerosis disability. Ann. Neurol. 76, 568–580.
Schmidt, P., Gaser, C., Arsic, M., Buck, D., Förschler, A., Berthele, A., Hoshi, M., Ilg, R., Schmid, V.J., Zimmer, C., Hemmer, B., Mühlau, M., 2012. An automated tool for detection of FLAIR-hyperintense white-matter lesions in Multiple Sclerosis. Neuroimage 59, 3774–3783.
Schmierer, K., Scaravilli, F., Altmann, D.R., Barker, G.J., Miller, D.H., 2004. Magnetization transfer ratio and myelin in postmortem multiple sclerosis brain. Ann. Neurol. 56, 407–415.
Smith, S.M., Zhang, Y., Jenkinson, M., Chen, J., Matthews, P.M., Federico, A., De Stefano, N., 2002. Accurate, robust, and automated longitudinal and cross-sectional brain change analysis. Neuroimage 17, 479–489.
Valsasina, P., Rocca, M.A., Horsfield, M.A., Absinta, M., Messina, R., Caputo, D., Comi, G., Filippi, M., 2012. Regional Cervical Cord Atrophy and Disability in Multiple Sclerosis: A Voxel-based Analysis. Radiology.